Chirality-dependent boron-mediated growth of nitrogen-doped single-walled carbon nanotubes

Joseph G. Wiltshire, Lain-Jong Li, Laura M. Herz, and Robin J. Nicholas*
Department of Physics, Oxford University, Parks Road, Oxford OX1 3PU, United Kingdom

Marianne Glerup† and Jean-Louis Sauvajol
GDPC (UMR5581), Universite Montpellier II, Place E. Bataillon, 34095 Montpellier Cedex 5, France

Andrei N. Khlobystov
Department of Materials, Oxford University, Parks Road, Oxford OX1 3PH, United Kingdom
(Received 23 May 2005; revised manuscript received 1 August 2005; published 21 November 2005)

A change in the relative abundance of single-walled carbon nanotubes, due to the presence of both nitrogen and boron during synthesis, has been identified through Raman and absorption spectroscopy. Raman spectroscopy shows that for two specific branches boron mediates the growth of smaller-diameter zigzag or near-zigzag nanotubes. We combine our experimental results with an improved Kataura model to identify two of the preferentially grown species as (16,0) and (14,1).

DOI: 10.1103/PhysRevB.72.205431 PACS number(s): 81.07.De, 78.30.Na, 78.55.−m, 61.46.+w

I. INTRODUCTION

Several single-walled carbon-nanotube- (SWNT-)based structures have recently been reported that demonstrate the tuning of the electronic properties of nanotubes through intermolecular charge transfer, brought about by the insertion of metallocenes[1] and endohedral metallofullerenes[2] or the intercalation of inorganic molecules.[3] The introduction of heteroatoms such as boron or nitrogen into the nanotube lattice, either as part of the synthesis process,[4,5] or in a postproduction substitution reaction,[6] is also predicted to modify the electronic properties of carbon nanotubes,[7] and offers the potential combination of doping the nanotubes with increased oxidation resistance.[8] However, there are also predicted to be strong physical effects due to the presence of these dopants during synthesis.[5,9] Here, we present a detailed study of the effects on the diameter distribution, relative populations, and electronic band gaps of semiconducting SWNTs produced by a modified arc-discharge process, where the anode is doped with various concentrations of both boron and nitrogen and show that boron has the dominant effect on the growth processes during synthesis.

Gai *et al.* reported the morphological effects of boron doping Co:Ni graphite targets used in the laser ablation synthesis of nanotubes.[5] Targets with low boron concentrations (<3.5 at. %) produced SWNTs without any detectable boron atoms incorporated. Above this level the presence of boron significantly altered the nanostructure of the sample material, resulting initially in the production of defective graphitic layers with a small fraction of double-walled nanotubes (DWNTs). Although no incorporated boron was found [above the electron energy loss (EEL) spectra detection limit of 0.05–0.1 at. %] its presence in the target clearly had an appreciable effect on the growth mechanisms during synthesis. Glerup *et al.* recently demonstrated that it is possible to grow nitrogen-doped SWNTs using composite anodes in a modified arc-discharge process.[4] The incorporation of sp^2-type bonded nitrogen was nominally measured as 1 at. % as determined by EEL spectra.

Studies to date have concentrated on the structural changes produced by boron or nitrogen inclusion during synthesis. Here we focus on the low-doping regime (~1 at. % and less) where SWNT production still dominates. At low doping the fundamental band structure is expected to be unchanged relative to the all-carbon model.

II. EXPERIMENT

Experiments were carried out to synthesize single-walled CB_xN_y and CN_x nanotubes and compare these to undoped carbon nanotubes (sample 1). The direct current during production was 95–100 A, which is similar to standard arc-discharge experiments although the voltage was slightly lower than the optimized conditions used for the synthesis of pure SWNTs. Graphite (1–2 μm, Aldrich) and Ni-Y catalyst (Ni, 99.999%, ~100 mesh, Aldrich; Y, 99.9%, ~40 mesh, Aldrich; Ni=Y=0.6 wt %) was mixed with either boron nitride powder (99.8%, Matthey Reagents) or melamine ($C_3N_6H_6$, 99%, Aldrich) and packed into the drillings of the anode rods. Boron nitride corresponding to 1:1 and 4:4 at. % boron and nitrogen was used to produce the CB_xN_y materials (denoted samples 2 and 3). A nitrogen content corresponding to 1 and 4 at. % (denoted samples 4 and 5) was used for the CN_x synthesis. These sample preparation conditions are summarized in Table I. The nitrogen content in sample 3 was measured to be around 1 at. % which is

TABLE I. Sample names and preparation parameters.

Sample name	Prepared dopant concentration
1	Undoped
2	1:1 at. % B:N
3	4:4 at. % B:N
4	1 at. % N
5	4 at. % N

close to the EELS detection limit.[4] No boron was detected in either sample 2 or 3 within the detection limit of ~0.1 at. %. Detailed studies of the synthesis of these samples have already been reported.[4]

High-resolution transmission electron microscopy (HRTEM) was performed using a JEOL JEM-4000EX LaB_6 microscope at room temperature and at an accelerating voltage of 100 kV. Samples were prepared by ultrasonicating a disperson of ~0.005 mg of the sample material in 2 ml of MeOH for 15 min. This dispersion was then deposited onto copper TEM grids coated with a carbon film (Agar).

Raman spectroscopy of the doped and undoped samples was performed in a backscattering geometry at 300 K using the 488 and 515 nm excitations of an Ar^+ laser and a Jobin-Yvon T64000 spectrometer with a liquid-nitrogen-cooled charge-coupled device. Each sample was prepared by ultrasonicating ~0.005 mg of the SWNT material in ~3 ml of MeOH for 40 min before placing a drop of the MeOH-SWNT suspension onto a Si substrate. This was then dried in an oven at 70 °C for 1 h.

Samples for optical absorption were prepared by depositing thin films of carbon nanotubes onto ZnSe substrates. This was achieved by ultrasonicating the SWNT material in MeOH for 30–45 min, and spraying the resulting solution onto the substrate using a modified Badger 200NH airbrush. To aid the evaporation of the MeOH the sample was heated to 150 °C during airbrushing using a Corning P-35 hotplate. Absorption spectra were obtained using a Perkin Elmer Lambda 9 Spectrophotometer.

III. RESULTS

HRTEM images of doped samples 2 and 3 are given in Fig. 1 which show nanotube diameters of 1.1–1.5 nm, which is typical for arc-discharge production. Despite the doping the tubular structure remains intact, although an increase in amorphous and partially graphitized material was observed. The TEM images do not show any defective structures such as double-walled carbon nanotubes or bamboolike nanostructures, associated previously with high boron doping.[5,6]

Raman spectra for the undoped, nitrogen- (N-), and boron- and nitrogen- (BN-)doped samples are shown in Fig. 2, for the region of the radial breathing mode (RBM) and are representative of the results from ~10 different locations. Figure 2 confirms the presence of nanotubes with diameters between 1.15 and 1.58 nm, as calculated by fitting Lorentzian peaks to the individual RBM modes and using the empirically deduced relationship between diameter and Raman shift, which includes the effects of van der Waals interactions between nanotubes.[10] These fitting values are summarized in Table II along with the E_{11}^S energies predicted from the Bachilo *et al.* model.[11] Small differences are present between the theoretical and fitted values due to a combination of the error in the calibration and its drift over the time of the experiment as well as the errors in the fitting procedure due to the presence of an underlying silicon substrate feature at 200–450 cm^{-1} and the finite linewidth of the peaks. Previous Raman spectroscopic studies[12] suggest that, for nanotubes in the diameter region of 1.2–1.6 nm, Raman excitation at 488 and 515 nm will resonantly excite predominantly semiconducting tubes that have resonances with the E_{33}^S transition energies. The predicted E_{11}^S energies agree well with the absorbance spectra shown in Fig. 3. Our results demonstrate that there is a dramatically different effect on the properties of the nanotubes when doping with boron and nitrogen compared with nitrogen alone. Figure 2 shows that there is very little change in the diameter distribution produced by nitrogen doping whereas with increasing boron and nitrogen doping of the anode there is a rapid change in Raman intensity toward peaks corresponding to nanotubes with smaller diameters. Deviations in the Raman shifts for the individual component lines between the undoped and BN-doped samples are smaller than 1.6 cm^{-1}, i.e., below the spectrometer calibration and peak fitting errors. There is therefore no appreciable change in the diameters of any of the individual species present, which might have led to changes in the resonance conditions. This agrees with the results of McGuire *et al.* who reported Raman spectra of boron-doped nanotubes.[13] Instead changes in the RBM spectra must result from changes in the relative abundance of the different nanotube species. It is also possible that the incorporation of dopants may alter the band gap independently of diameter and hence affect the resonant coupling with the incident laser photons, a possibility which is further discussed in the following section.

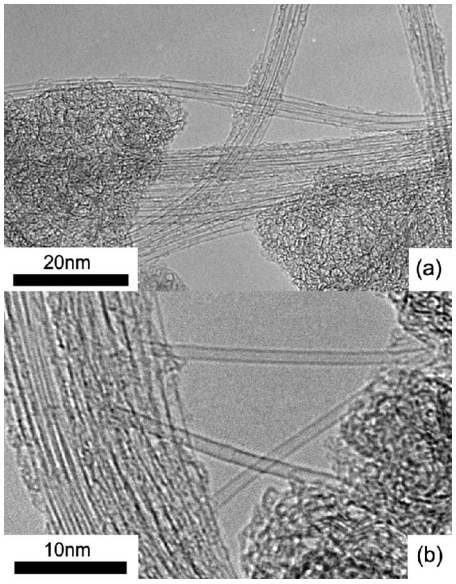

FIG. 1. HRTEM images of (a) BN-doped sample 2 and (b) BN-doped sample 3. These images show both isolated nanotubes and small bundles with nanotube diameters 1.1–1.5 nm. They demonstrate that the doping of the anode during arc-discharge synthesis has not significantly diminished the tubular structure.

We now discuss the band gaps of the semiconducting nanotubes as deduced from the background-corrected absorbance spectra shown in Fig. 3. These show the E_{11}^S and E_{22}^S modes with centers at 0.71 and 1.25 eV, respectively, for the undoped nanotubes. These are a superposition of the electronic transitions between the first and second van Hove singularities in the density of states for the individual semicon-

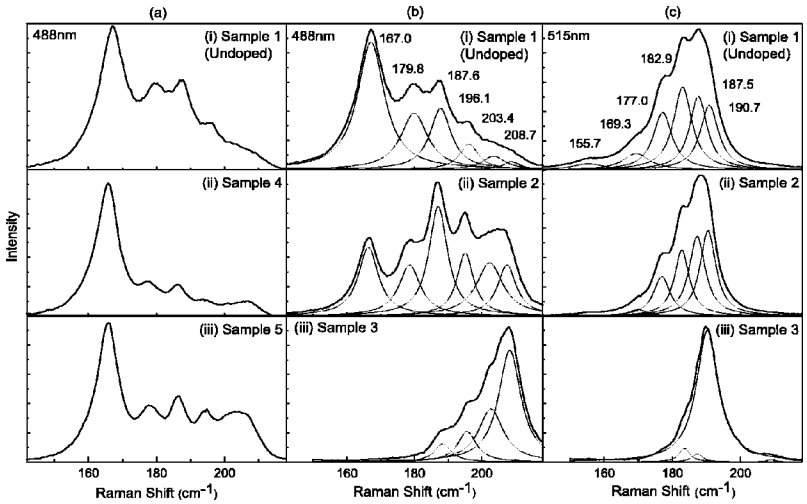

FIG. 2. RBM spectra using the (a) 488 nm excitation wavelength for samples (i) undoped sample 1, (ii) N-doped sample 4, and (iii) N-doped sample 5; (b) 488 nm excitation wavelength for samples (i) undoped sample 1, (ii) BN-doped sample 2, and (iii) BN-doped sample 3; (c) 515 nm excitation wavelength for samples (i) undoped sample 1, (ii) BN-doped sample 2, and (iii) BN-doped sample 3. Peak fitting was performed using a Lorentzian line shape and a linear background.

ducting nanotubes. As the absorption process is nonresonant, the spectra should represent an unbiased average over the full distribution of semiconducting nanotube diameters, but should relate to the RBM spectra which are also predicted to be mainly from semiconducting tubes. For the undoped sample the E_{11}^S and E_{22}^S values correspond to a mean diameter of $\sim$1.4 nm consistent with the values deduced from the RBM modes. As BN doping in the anode is increased the average E_{11}^S mode energy increases, which we also attribute to changes in the populations of the various species, in favor of smaller-diameter nanotubes, e.g., for sample 3 E_{11}^S =0.78 eV which implies a mean diameter of $\sim$1.3 nm. The E_{22}^S mode contains two distinct contributions at $\sim$1.2 and $\sim$1.3 eV which follow a similar trend. As doping is increased the relative intensity of the lower-energy feature, corresponding to larger diameter nanotubes, decreases relative to the feature at 1.3 eV, until in sample 3 the feature is not present. This development occurs in tandem with a further increase in absorption on the higher-energy side.

The changes to the E_{11}^S and E_{22}^S modes correspond well with the evolution of the individual species in Fig. 2. We conclude that these are not due to doping or other modifications to the electronic structure caused by the exchange of electrons from the nitrogen or boron heteroatoms, since these would only suppress electron transitions for E_{11}^S by changing the Fermi energy;[14] however, the E_{22}^S absorption would be largely unaffected.[15,16] The fact that the same behavior is observed for both E_{11}^S and E_{22}^S suggests that the effect is due to relative changes in the abundance of the species, in favor of smaller nanotubes.

TABLE II. Fitted parameters for the RBM of samples 1, 2, and 3, for the 488 and 515 nm laser wavelengths. Also contained are the predicted E_{11}^S energies for the given n and m indices adapted from the Bachilo *et al.* model (Ref. 11).

d[a] (nm)	ω_{RBM} (cm^{-1}) 1	2	3	(n,m) predicted	Predicted ω_{RBM} (cm^{-1})[a]	Bachilo *et al.* E_{11}^S (eV)
			488 nm excitation			
1.46	167.0	166.2				
1.35	179.8	178.4				
1.30	187.6	186.9	188.3	10,9	185.4	0.794
1.25	196.1	194.9	195.5	11,7	193.4	0.812
1.20	203.4	202.2	202.6	12,5	200.4	0.827
1.15	208.7	207.4	208.2	14,1	208.2	0.828
			515 nm excitation			
1.58	155.3					
1.44	169.3	169.7		11,10	169.1	0.727
1.38	177.0	176.8		12,8	175.8	0.743
1.34	182.9	182.6	183.4	13,6	181.7	0.761
1.30	187.5	187.1	187.2	14,4	186.3	0.764
1.27	190.7	190.3	190.2	16,0	190.3	0.765

[a]Calculated from the undoped sample using $d=224/(\omega_{RBM}-14)$ with an $a_{C-C}=0.144$ nm (Ref. 10).

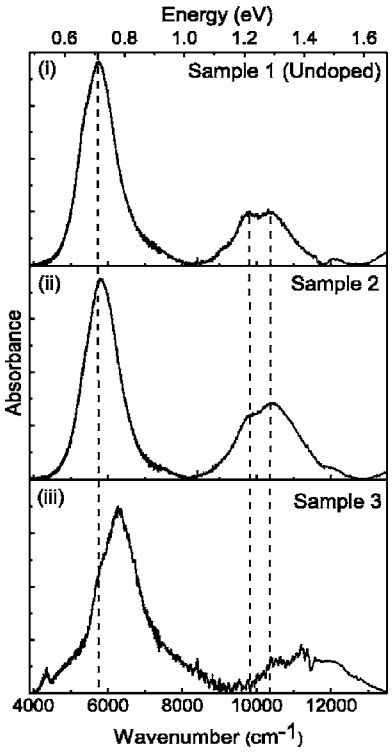

FIG. 3. Background-adjusted absorbance spectra of the E_{11}^S and E_{22}^S modes for the (i) undoped sample 1, (ii) doped sample 2, and (iii) doped sample 3.

IV. DISCUSSION

Nitrogen incorporation in multiwalled carbon nanotubes (MWNTs) is routinely reported above 10 at. %,[17,18] whereas only a few percent has ever been reported for boron-doped MWNTs.[19] This is supported by the fact that for our samples nitrogen was nominally measured at 1 at. % while no sp^2-type bonded boron was detected. Molecular dynamics simulations have shown that it is favorable for boron to remain at the growth edge of a zigzag nanotube or one bond from the edge in the case of armchair nanotubes.[20,21] Therefore for zigzag nanotubes, boron would be expected to concentrate at the growth edge, where it can have a strong influence on the growth processes. These simulations predicted that boron acts to reduce the number of dangling bonds at the growth edge, preventing tip closure and mediating the growth of longer zigzag nanotubes. Furthermore Blase *et al.* found no boron heteroatoms in the body of their nanotubes, within their detection limit of ~1 at. %; however, boron was found at the tips of their nanotubes, as would be predicted by the simulations.[20]

We identify the chiral indices of the tubes present from the resonant excitations predicted by a Kataura plot for the E_{33}^S band gaps. The parameters for an accurate description of E_{33}^S have not yet been fully established so the plots we present here have been based on fitting the expressions used by Strano *et al.* which take account of the effects of chirality[22] (trigonal warping) to deduce the shifts in the band gap energies from the simple armchair (n,n) case. The values for the fitting parameters for E_{33}^S were derived from the

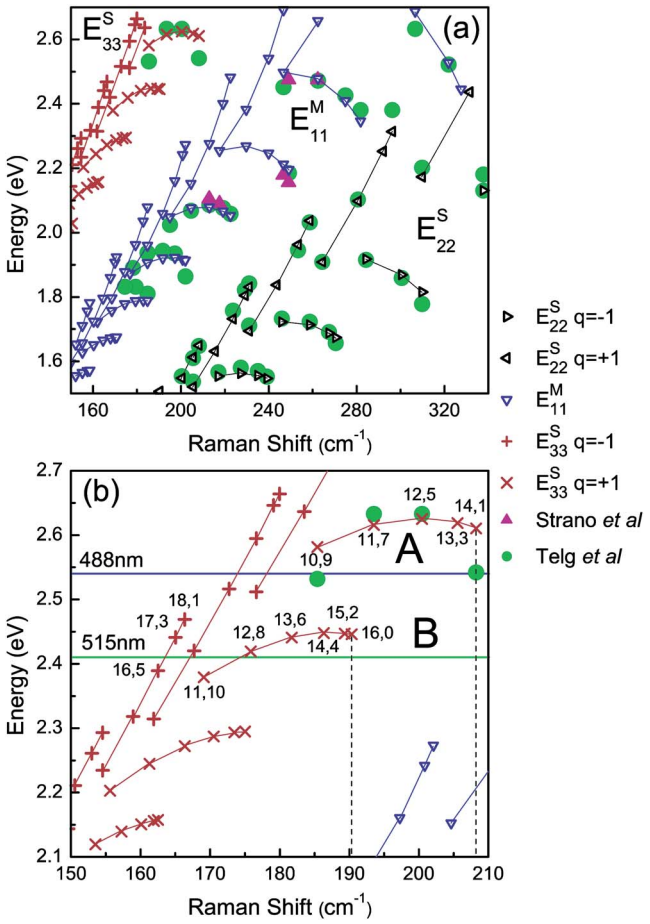

FIG. 4. (Color online) Kataura plot of energy against Raman shift of the radial breathing mode. In (a) the second (E_{22}^S) and third (E_{33}^S) transitions for semiconducting nanotube species are shown along with the first transition (E_{11}^M) for the metallic nanotubes. (b) An expanded version of the area of interest of the E_{33}^S transition, shown with the relevant n,m assignments and the laser excitation wavelengths. Both figures include experimental data adapted from Refs. 23 and 24.

preliminary data reported by Lebedkin *et al.* for photoluminescence (PL) excitation maps[23] while the fitting parameters for the E_{22}^S and E_{11}^M were derived from the resonant Raman spectra of both Strano *et al.*[22] and Telg *et al.*[24] Details of the parameters used are available in the supplementary information.[25]

The Kataura model is replotted in terms of expected Raman shift in Fig. 4, with a magnification of the E_{33}^S band in the region of interest. It shows two branches labeled *A* and *B* which are close to resonance with the 488 and 515 nm laser wavelengths, respectively. These shallow $q=+1$ branches both correspond to semiconducting nanotubes with a nearly constant resonant excitation, where $n-m=3p+q$ and p is an integer and $q=\pm 1$. Recent reports have shown that the phonon-photon interaction for semiconducting nanotubes is chirality dependent.[26] In particular the cross section for the RBM is dependent on the sign of q and which band gap is close to the excitation energy. Doorn *et al.*[27] measured high RBM intensities from $q=-1$ species when excited close to their E_{22}^S band gap, suggesting that for E_{33}^S the $q=+1$ species

will have higher RBM intensities, corresponding to the dominant features shown in Fig. 2.

The end species on branches *A* and *B* have predicted Raman shifts of 208 and 190 cm^{-1}, which are in good agreement with the frequencies observed in Fig. 2 of 209 and 191 cm^{-1} for excitation wavelengths of 488 and 515 nm, respectively. However, due to the finite linewidths of the peaks the penultimate species in each branch, which have predicted RBM frequencies only $1-3$ cm^{-1} different from the assigned nanotubes, are also possible candidates. The other assignments in Table II are unlikely to overlap with other species as few candidates exist within their respective resonance windows. No assignment of the lowest frequencies in the Raman spectra is made because of the presence of the E_{33}^S $q=-1$ branch and also the proximity of the E_{44}^S band (not shown). Small changes in the parameters used in the model would lead us to assign different species in the $q=-1$ branch. The experimental values in Table II agree well with the predicted branches *A* and *B* which show that as one moves out from the root of either branch toward the tip the chiral angle reduces until the final species in branch *B* is a zigzag nanotube (16,0) and in branch *A* it is a (14,1). These two nanotubes give dominant signals in the Raman spectra of the highest BN-doped sample. This assignment supports previous proposals that the presence of boron during synthesis preferentially mediates the growth of zigzag or near-zigzag species, to the exclusion of the other chiralities. It should be noted that a lower chiral angle also corresponds to a smaller diameter for branches *A* and *B*, and so a diameter-dependent mediated growth cannot be ruled out as an explanation of our experimental results; however, no curvature dependence was predicted in the growth simulations as the calculated energies were found to be similar for tubules and planar sheets of graphene, although the simulations did not include the interaction between boron and the metal catalysts at the growth edge.

V. CONCLUSIONS

Many recent developments in the manufacturing of doped nanostructures have been reported and nitrogen- and boron-doped nanotubes represent just some of many candidates. Although boron is more difficult than nitrogen to include in the lattice structure we have shown that it has a strong effect on the growth of nanotubes. This may allow for longer nanotubes to be grown between electrodes in device manufacturing. Finally a narrowing of the diameter distribution, in favor of smaller-diameter zigzag or near-zigzag nanotubes, has been measured by Raman spectroscopy. Optimizing this process will lead to a natural counterpart to recently developed armchair-rich materials[28] so that chirality-dependent studies can more easily be made. Improved control of the chiral angle of bulk nanotube material may have applications for future photoluminescence and Raman experiments where deconvolved features are needed.

ACKNOWLEDGMENTS

Parts of this work were funded by EPSRC. A.N.K. thanks the Leverhulme Trust and the University of Nottingham. M.G. acknowledges Contract No. HPRN-CT-2000-00157 for funding. L.J.L. thanks the Swire Group for financial support.

*Electronic address: r.nicholas@physics.ox.ac.uk
†Also at Grenoble High Magnetic Field Laboratory, 25 Avenue des Martyrs, 38042 Grenoble, Cedex 9, France and Department of Chemistry, University of Oslo, P.O. Box 1033, Blindern, 0315 Oslo, Norway.

[1] L. J. Li, A. N. Khlobystov, J. G. Wiltshire, G. A. Briggs, and R. J. Nicholas, Nat. Mater. **4**, 481 (2005).
[2] J. Lee, H. Kim, S. J. Kahng, G. S. G. Kim, J. Ihm, H. Kato, Z. W. Wang, T. Okazaki, H. Shinohara, and Y. Kuk, Nature (London) **415**, 1005 (2002).
[3] C. Zhou, J. Kong, E. Yenilmez, and H. Dai, Science **290**, 1552 (2000).
[4] M. Glerup, J. Steinmetz, D. Samaille, O. Stéphan, S. Enouz, A. Loiseau, S. Roth, and P. Bernier, Chem. Phys. Lett. **387**, 193 (2004).
[5] P. L. Gai, O. Stephan, K. McGuire, A. M. Rao, M. S. Dresselhaus, G. Dresselhaus, and C. Colliex, J. Mater. Chem. **14**, 669 (2004).
[6] D. Golberg, Y. Bando, L. Bourgeois, K. Kurashima, and T. Sato, Carbon **38**, 2017 (2000).
[7] M. Terrones, A. Jorio, M. Endo, A. M. Rao, Y. A. Kim, T. Hayashi, H. Terrones, J. C. Charlier, G. Dresselhaus, and M. S. Dresselhaus, Mater. Today **7**, 1 (2004).
[8] T. Belz, A. Baue, J. Find, M. Günter, D. Herein, H. Möckel, N. Pfänder, H. Sauer, G. Schulz, and J. Schütze, Carbon **36**, 731 (1998).
[9] R. Droppa, P. Hammer, A. C. M. Carvalho, M. C. dos Santos, and F. Alvarez, J. Non-Cryst. Solids **299**, 874 (2002).
[10] A. M. Rao, J. Chen, E. Richter, U. Schlecht, P. C. Eklund, R. C. Haddon, U. D. Venkateswaran, Y. K. Kwon, and D. Tománek, Phys. Rev. Lett. **86**, 3895 (2001).
[11] S. M. Bachilo, M. S. Strano, C. Kittrell, R. H. Hauge, R. E. Smalley, and R. B. Weisman, Science **298**, 2361 (2002).
[12] A. Jorio, R. Saito, J. H. Hafner, C. M. Lieber, M. Hunter, T. McClure, G. Dresselhaus, and M. S. Dresselhaus, Phys. Rev. Lett. **86**, 1118 (2001).
[13] K. McGuire, N. Gothard, P. L. Gai, M. S. Dresselhaus, G. Sumanasekera, and A. M. Rao, Carbon **43**, 219 (2005).
[14] L.-J. Li and R. J. Nicholas, Nanotechnology **15**, 1844 (2004).
[15] N. Minami, S. Kazaoui, R. Jacquemin, H. Yamawaki, K. Aoki, H. Kataura, and Y. Achiba, Synth. Met. **116**, 405 (2001).
[16] T. Takenobu, T. Takano, M. Shiraishi, Y. Murakami, M. Ata, H. Kataura, Y. Achiba, and Y. Iwasa, Nat. Mater. **2**, 683 (2003).
[17] S. Trasobares, O. Stéphan, C. Colliex, W. K. Hsu, H. W. Kroto, and D. R. M. Walton, J. Chem. Phys. **116**, 8966 (2002).
[18] M. Glerup, M. Castignolles, M. Holzinger, G. Hug, A. Loiseau, and P. Bernier, Chem. Commun. (Cambridge) **20**, 2542 (2003).
[19] P. Redlich, J. Loeffler, P. M. Ajayan, J. Bill, F. Aldinger, and M.

Rühle, Chem. Phys. Lett. **260**, 465 (1996).
[20] X. Blase, J. C. Charlier, A. D. Vita, R. Car, P. Redlich, M. Terrones, W. K. Hsu, H. Terrones, D. L. Carroll, and P. M. Ajayan, Phys. Rev. Lett. **83**, 5078 (1999).
[21] E. Hernández, P. Ordejón, I. Boustani, A. Rubio, and J. A. Alonso, J. Chem. Phys. **113**, 3814 (2000).
[22] M. S. Strano, S. K. Doorn, E. H. Haroz, C. Kittrell, R. H. Hauge, and R. E. Smalley, Nano Lett. **3**, 1091 (2003).
[23] S. Lebedkin, K. Arnold, F. Hennrich, R. Krupke, B. Renker, and M. M. Kappes, New J. Phys. **5**, 140 (2003).
[24] H. Telg, J. Maultzsch, S. Reich, F. Hennrich, and C. Thomsen, Phys. Rev. Lett. **93**, 177401 (2004).
[25] See EPAPS Document No. E-PRBMDO-72-063544 for a description of the equations and model parameters used for the Kataura plot. This document can be reached via a direct link in the online article's HTML reference section or via the EPAPS homepage (http://www.aip.org/pubservs/epaps.html).
[26] R. Saito, A. Jorio, J. H. Hafner, C. M. Lieber, M. Hunter, T. McClure, G. Dresselhaus, and M. S. Dresselhaus, Phys. Rev. B **64**, 085312 (2001).
[27] S. K. Doorn, D. A. Heller, P. W. Barone, M. L. Usrey, and M. S. Strano, Appl. Phys. A: Mater. Sci. Process. **78**, 1147 (2004).
[28] S. M. Bachilo, L. Balzano, J. E. Herrera, F. Pompeo, D. E. Resasco, and R. B. Weisman, J. Am. Chem. Soc. **125**, 11186 (2003).